Carbon 145 (2019) 677–689

Contents lists available at ScienceDirect

Carbon

journal homepage: www.elsevier.com/locate/carbon

Bio-inspired, nitrogen doped CNT-graphene hybrid with amphiphilic properties as a porous current collector for lithium-ion batteries

Yu-Yun Hsieh [a], Yanbo Fang [a], Jeremy Daum [b], Sathya Narayan Kanakaraj [a], Guangqi Zhang [a], Siddharth Mishra [a], Seyram Gbordzoe [a], Vesselin Shanov [a, b, *]

[a] Department of Mechanical and Materials Engineering, University of Cincinnati, Cincinnati, OH, 45221-0072, USA
[b] Department of Chemical and Environmental Engineering, University of Cincinnati, OH, 45221-0012, USA

ARTICLE INFO

Article history:
Received 7 November 2018
Received in revised form
27 December 2018
Accepted 16 January 2019
Available online 19 January 2019

ABSTRACT

Carbon-based materials have been proposed as current collectors for lithium ion batteries (LIBs), however few of them have successfully integrated sp^2 carbon and reach in sp^3 carbon into one monolithic structure: in a way that sp^2 carbon is responsible for electron transfer and sp^3 carbon is capable for a high loading of active materials. Here we report an in-situ growth of a nitrogen-doped carbon nanotube (NCNT) on a three-dimensional (3D) graphene network. The proposed structure (NCNT-3DG) is a bio-inspired nanomaterial with a design of a "natural forest". The in-situ growth of NCNT on 3D graphene guarantees a fast electron transfer between NCNT and 3DG. The hydrophilic nature of NCNTs insures a high loading of the active materials, such as $Li_4Ti_5O_{12}$ (LTO). The designed LTO-NCNT-3DG electrode achieves an active materials loading of 74 wt% of the overall electrode mass, compared to about 20 wt% on traditional metal foil and 55 wt% on other reported carbon current collectors. Such a hybrid electrode delivers a higher specific capacity of 158 mAh g^{-1} at 5C. The specific capacity retains 94% after 2000 cycles at 10 C. The proposed NCNT-3DG current collector is a novel strategy for fast charging LIBs.

1. Introduction

Lithium ion batteries (LIBs) with fast charging capability received a lot of attentions due to the fast development of electric-vehicles and renewable energy sources [1,2]. However, the fast charging LIBs also face challenges such as low energy density, low charging efficiency and safety concerns [3]. It is well known that the rate performance of an LIB is largely related to the ionic and electronic transport kinetics of the electrode material used in the LIB [4,5]. To address these challenges, many efforts have been devoted to research and development of high power anode or cathode materials [6–8], safe electrolytes [9] and advanced separators [10,11]. Unfortunately, less attention has been paid to study next generation current collectors, which indeed can help improving the rate performance of LIBs. An ideal current collector for a fast charging LIBs, is expected to reveal properties such as high electrical conductivity, good electrochemical stability, lightweight, mechanical robustness, and high loading capacity of the battery active materials. These merits could potentially decrease the overall mass of the battery cell and reduce the overall resistance, resulting in an improved energy density and power density of the battery cell and in a safer device. Based on the configuration of traditional current collectors, the plausible way to achieve fast charging capability is to either reduce the active materials loading by thin-coating, or to shrink the length of lithium ion diffusion pathway through nano-engineering. Nonetheless, both approaches show their limitations in achieving a high loading of active materials. For example, increasing the loading of active materials results in an impeded electron transport between the active materials and the current collector. Nano-sized active materials also tend to agglomerate in order to reduce the surface energy [4], especially in high loading where chances are higher for one nanoparticle to contact with others.

Recently, porous current collectors have been proposed to improve the electrical conductivity of the overall electrode by shortening the electron pathway between the active materials and the current collectors [12–15]. Carbon materials such as carbon nanotubes (CNTs) [16,17], graphene [6–8,18], and graphene-CNT hybrid [19–23] have demonstrated great promise for this

* Corresponding author. Department of Mechanical and Materials Engineering, University of Cincinnati, Cincinnati, OH, 45221-0072, USA.
E-mail address: vesselin.shanov@uc.edu (V. Shanov).

https://doi.org/10.1016/j.carbon.2019.01.055
0008-6223/

application. Compared to their metal counterparts, carbon-based current collectors are lightweight, porous and flexible. However, they either lack of high electrical conductivity due to the highly defective structure (especially in chemically derived graphene oxide) bearing high junction contact resistance, or they have a low active materials mass loading due to the unfavorable surface energy of their low-defect structure to active materials (known for graphene synthesized by chemical vapor deposition (CVD)). In fact, it is a challenge to concurrently obtain high electrical conductivity and high mass loading of the active materials by using a single carbon material, which atoms are usually either sp^2 or sp^3 bonded domain. For the carbon with sp^2 bonding domain structure (such as good quality graphene or metallic carbon nanotubes), a high electrical conductivity is expected [24,25]. However, the hydrophobic nature of such a structure prevents it from interacting with battery active materials, which are mostly hydrophilic. This leads to a low mass loading and non-uniform distribution of the active battery materials [26]. On the other hand, the carbon with sp^3 bonding domain structure provides active sites to achieve a high loading of the battery active materials, but the poor electrical conductivity of sp^3 carbon hinders such materials to achieve a high rate performance [27]. Therefore, it is reasonable to believe the integration of two or more types of carbon materials, each with either sp^2 and sp^3 bonding, can achieve high electrical conductivity and high mass loading of active materials at the same time. It is also important to insure the contact resistance between different carbon structures remains minimum. This will enable seamless contact between different carbon materials (by in-situ grown of one on the another), thus making such an approach more favorable than simple physical mixing of different materials.

Herein, we propose a nitrogen-doped CNT-three-dimensional graphene (NCNT-3DG) hybrid structure with amphiphilic (hydrophobic and hydrophilic features within the same structure) and bio-inspired features, working as a current collector for loading the battery active materials. Here, we use $Li_4Ti_5O_{12}$ (LTO) to exemplify the potential of the proposed hybrid structure. LTO is considered a good anode materials candidate for fast-charging LIBs, because it has excellent cyclability with almost no volume expansion during the process of lithiation[28–30]. Moreover, its high operating voltage, i.e. 1.55 V (vs Li/Li+), makes it safe for high current rates as compared to graphite operating around 0.1 V [30]. However, LTO suffers from a low electrical conductivity ($<10^{-13}$ S cm^{-1}) at room temperature [31], therefore the NCNT-3DG current collector is proposed to address this issue. The distinctive differences between this proposed hybrid structure and other CNT/Graphene composites are: (1) The 3DG is a monolithic structure that ensures a fast long-range electron transfer. It also contributes to a good mechanical robustness that allows the 3DG to be used in a free-standing form. In such a configuration, the current collector, binder, and conductive additives that are used in traditional electrode design are embedded into one free-standing 3DG structure, allowing for an easy electrode fabrication; (2) NCNT assembling with the 3DG is achieved by in-situ CVD growth, thus the contact resistance between NCNT and 3DG is expected to substantially reduced compared to hybrid materials prepared by simple physical mixing; (3) Unlike other carbon current collectors prepared by filtration [7,19,22,23], the great porosity of the proposed hybrid structure enables a high loading of battery active materials without a risk of delamination. The studied in this work NCNT-3DG current collector has a lightweight nature (areal density of 0.7 mg cm^{-2}) compared to the commonly used metal current collectors (Al ~ 7 mg cm^{-2} and Cu ~ 8 mg cm^{-2}). The proposed hybrid carbon structure employed as a current collector in LIBs allows to achieve a high ratio of active materials loading (ratio of the mass of active materials to the mass of the overall electrode). This approach helped us to solve simultaneously the issues with high interfacial resistance and low mass loading of active materials found in traditional current collector and other reported carbon current collectors. All this makes the proposed hybrid electrode very promising to be a novel strategy for fast ions and electrons transfer in high power LIB with an improved mass loading of active materials.

2. Experimental section

2.1. Synthesis of nitrogen-doped carbon nanotubes-three-dimensional graphene (NCNT-3DG) hybrid structure, and of carbon nanotubes-three-dimensional graphene (CNT-3DG)

High quality (sp^2-bonding domain) 3D graphene (3DG) was synthesized through a chemical vapor deposition (CVD) process, which was described elsewhere [32]. A mixture of 5.5 g polystyrene (Sigma Aldrich, 210000 M W.), plasticizer diethylene glycol dibenzoate (DEGD, Sigma Aldrich) (1.75 mL), 40 g nickel powder, and 40 mL toluene was prepared as a slurry and knife-cast to make a nickel powder/polymer thin film as a CVD catalyst precursor for synthesis of 3DG. The 3DG was then used as a substrate to synthesize nitrogen-doped CNT with defects having sp^3-nature. $NiCo_2O_4$ flake-like nanostructures and acetonitrile (C_2H_3N) were used as catalyst and precursor, respectively, for CVD synthesis of nitrogen-doped CNT at 780 °C. The $NiCo_2O_4$ nanoflakes were anchored on the 3DG by air annealing the obtained nickel-cobalt binary hydroxide (NiCoOH) synthesized through a solvothermal process. This procedure included first preparation of a mixture consisted of 0.6 mmol of $Ni(NO_3)_2 \cdot 6H_2O$, 1.2 mmol of $Co(NO_3)_2 \cdot 6H_2O$, and 1.8 mmol of urea dissolved in different ratio of ethanol aqueous solution (pure DI water, DI water:ethanol = 4:1, and pure ehanol) (40 mL). Then, the 3DG was immersed in the solution and then sealed in a Teflon-lined stainless-steel autoclave for conducting a solvothermal reaction at 126 °C that lasted 3 h forming NiCoOH compound. After this, the 3DG with NiCoOH were air annealed at 350 °C for 5 min to transfer NiCoOH into $NiCo_2O_4$ nanoflakes. Synthesis of nitrogen doped CNTs on the 3DG was conducted in a tube furnace (FirstNano, ET1000). The produced $NiCo_2O_4$-3DG was heated up to 780 °C under Ar (1000 sccm), then, 100 sccm of C_2H_3N was introduced for 60 min. Lastly, the sample was cooled down to room temperature at a rate of ~100 °C min^{-1} under Ar (1000 sccm). The final N3DG-CNT was produced by etching out nickel and cobalt with a 3 M HCl at 60 °C for 12 h. The obtained NCNT-3DG hybrid material was washed with DI water to remove the residual acid. The procedures to synthesize the control sample of CNT-3DG were similar with those of practiced for NCNT-3DG, with one difference that ethylene was used as a carbon precursor instead of acetonitrile.

2.2. Synthesis of $Li_4Ti_5O_{12}$/NCNT-3DG (LTO-NCNT-3DG) and $Li_4Ti_5O_{12}$/3DG (LTO-3DG)

Both the 3DG and the NCNT-3DG are proposed here to work as current collector in anode. LTO-NCNT-3DG and LTO-3DG were prepared by a hydrothermal process [6]. In a typical procedure, 1.7 mL of 30% (wt/wt) hydrogen peroxide, 40 mL of 0.4 M LiOH, and 3 mmol of titanium tetraisopropoxide were mixed and stirred for 1 h. The NCNT-3DG and the 3DG were immersed in the mixture and then sealed in a 100 mL Teflon-lined stainless autoclave for conducting a hydrothermal reaction at 130 °C that lasted 12 h. After hydrothermal treatment, the as-prepared composites were washed with distilled water and then dried in an oven at 80 °C. The obtained composites were finally annealed at 550 °C for 6 h in argon.

2.3. Materials characterization

Scanning electron microscopy (SEM) (FEI XL30, 15 kV), Raman spectroscopy (Renishaw inVia, excited by a 514 nm Ar-ion laser with a laser spot size of ~1 μm^2), and TEM (FEI CM20, 300 kV) were used to characterize the 3DG, the NCNT-3DG, the LTO-3DG and the LTO-NCNT-3DG samples. Surface wettability of the 3DG and the NCNT-3DG were examined by using a contact angle instrument (Kruss, DSA100). Van der Pauw method (Keysight Technologies 34460A) was employed for electrical measurement of the samples [33]. Four terminals of the probe were slightly compressed on the surface of the samples having dimensions of 2 cm × 2 cm. The electrical conductivity was calculated based on the thickness of the samples, which were measured with a micrometer. X-ray photoelectron spectroscopy (XPS) (VG Thermo-Scientific MultiLab 3000 ultra-high vacuum surface analysis system) was done using an Al Kα source of 1486.6 eV excitation energy. The X-ray diffraction (XRD) patterns were collected using a Philips X'Pert Pro (PW3040/00, PANalytical) instrument with a step size 0.02° at 0.95 s/step. The scan range was set from 10° to 80° (in 2θ) with a Cu-tube operated at 45 kV and 40 mA. The mechanical tensile property was evaluated at 25 °C by using Instron 5948 testing instrument. The test samples were cut into 40 mm × 5 mm × ~0.05 mm band-like shape samples by laser and gripped by two pneumatic clips. The distance between two pneumatic clips was 25 mm and the strain rate was 1 mm min^{-1}.

2.4. Electrochemical performance measurements

The LTO-3DG and LTO-NCNT-3DG anodes were cut into circular pellets of 12 mm diameter and used as anodes without adding any conductive additives or binders. The loading mass of LTO was about 2 mg cm^{-2} for both LTO-3DG and LTO-NCNT-3DG. The electrolyte was prepared by mixing 1.0 M LiPF6 in ethylene carbonate/dimethyl carbonate (1:1 by volume). The volume of the electrolyte was 40 μL in all assembled cells. A 2032 type stainless steel coin cell was used to assemble a test cell. A lithium metal foil with a diameter of 15 mm was deployed as a counter electrode and microporous polypropylene film (Celgard, 2400) as a separator. The coin-type cell was assembled in an Ar-filled glovebox (Omni Lab, VAC). A galvanostatic charge-discharge instrument (BST8-MA MTI) was used to characterize the performance of the battery coin cell. Cyclic voltammetry (CV) studies were carried out on an electrochemistry workstation (Gamry, Interface 1000) from 1.0 V to 2.5 V at different scan rates. The coulombic rate set for cell tests was referred to the mass of LTO in the working electrode and varied from 0.5C to 30 C. The charge-discharge voltage range was in the range of 1.0–2.5 V. The electrochemical impedance spectroscopy (EIS) were conducted by using an electrochemical workstation (Gamry, Interface 1000) at room temperature and carried out at an open-circuit potential in the frequency range between 100 kHz and 0.01 Hz. All the capacity values were calculated based on the mass of LTO.

3. Results and discussion

3.1. Synthesis and characterization of NCNT-3DG

Conventional fabrication of electrodes for batteries requires metal current collectors such as Al/Cu foil used as a substrate in the slurry-casting process. However, the traditional metal current collector faces two main shortcomings (Fig. 1a). First, using metal current collector enlarges the electrons transporting distance between the metal current collector and the slurry layer of active materials. Second, a heavy metal current collector, resulting in a low active materials/the overall electrode (wt %), hardly contributes to the specific capacity of the whole cell. Therefore, a porous carbon current collector, as a freestanding 3DG material (Fig. 1b) without using any binder and conductive additive, is proposed to work here. Such a material behaves as a continuous, three-dimensional, strong mechanical scaffold which ensures a good long-range electrical conductivity [32,34]. However, despite the excellent electrical conductivity and good mechanical robustness of 3DG, it possesses a hydrophobic surface which creates difficulties to achieve a uniform dispersion of the active materials. The agglomeration of the active materials causes a longer ions diffusion length and a worse short-range electrical conductivity. The proposed amphiphilic NCNT-3DG hybrid material (Fig. 1c) shows advantages over the metal current collector and the 3DG, because it (i) prevents the agglomeration of active materials to shorten the ions diffusion length in the electrode by the hydrophilic nitrogen-doped CNT, (ii) increases the active materials loading per the overall electrode (wt %), and (iii) reduces the electrons transport length from the active materials to the overall conductive network by improved short-range electrical conductivity. Moreover, nitrogen (N) doping has higher electronegativity (3.5) compared to that of carbon (3.0), which is an effective way to increase electrical conductivity and wettability [35]. It is expected that N doping in NCNT-3DG structure can further improve the electronic conductivity and ions diffusion over the whole electrode structure. The thickness of 3DG and NCNT-3DG measured by a micrometer is about 15 μm after compressing by a hydraulic load of 1.13 MPa. The measured electrical conductivity of the NCNT-3DG (421 S cm^{-1}) is much higher than the pristine 3DG (265 S cm^{-1}). This indicates that the nitrogen doping playing a positive role to improve the electrical conductivity, which has also been observed by others [36–38]. The overall structure of the NCNT-3DG is bio-inspired and can be illustrated in Fig. 1d. The hydrophobic sp^2 bonding domain 3DG scaffold mimics the "forest's trunk roots" for long-term electron transfer over the whole structure, whereas the hydrophilic sp^3 bonding domain NCNT resembles the "crowns with branches of the trees within the forest" and serves as a platform for growth of battery active materials. The latter are compared here as "leaves".

The fabrication procedure used for the synthesis of the NCNT-3DG is illustration in Fig. 2a. First, the monolithic 3DG was prepare by CVD [32]. The obtained porous 3DG was immersed into an ethanol aqueous solution with $Ni(NO_3)_2 \cdot 6H_2O$ and $Co(NO_3)_2 \cdot 6H_2O$ for conducting a solvothermal reaction and forming a NiCoOH-3DG. The latter was dried, followed by calcinations in air to convert NiCoOH to $NiCo_2O_4$. The crystallographic structures of the 3DG, NiCoOH-3DG, and $NiCo_2O_4$-3DG were analyzed by XRD, as shown in Fig. S1. All three patterns revealed strong diffraction peak at 26.5° due to the presence of graphene flasks in the composite [8]. The diffraction peaks of the NiCoOH-3DG can be indexed as α-$Ni(OH)_2$ (JCPDS No. 38–715), and as α-$Co(OH)_2$. [39] The $NiCo_2O_4$-3DG can be indexed as spinel $NiCo_2O_4$ (JCPDS Card No. 20–0781) [40]. Finally, the NCNT-3DG hybrid structure was synthesized by CVD. The morphology of the "as-prepared" products during each preparation step have been studied by SEM and the results are displayed in Fig. 2a. The NCNTs occupy the void space within the 3DG structure, therefore, expected to increase surface area that is critical for high loading of active materials. To prove the increased hydrophilicity of the obtained hybrid material after the NCNT growth within the 3DG, we conducted a contact angle test for 3DG and NCNT-3DG using water droplets. As displayed in Fig. 2b, the measured contact angle of NCNT-3DG (59.2°) is smaller than that of 3DG (132°). This phenomenon indicates that NCNT-3DG samples are more compatible with aqueous solution which are used to synthesize active materials on the 3DG and NCNT-3DG. In addition, the nitrogen induced defects within in the CNTs provide higher

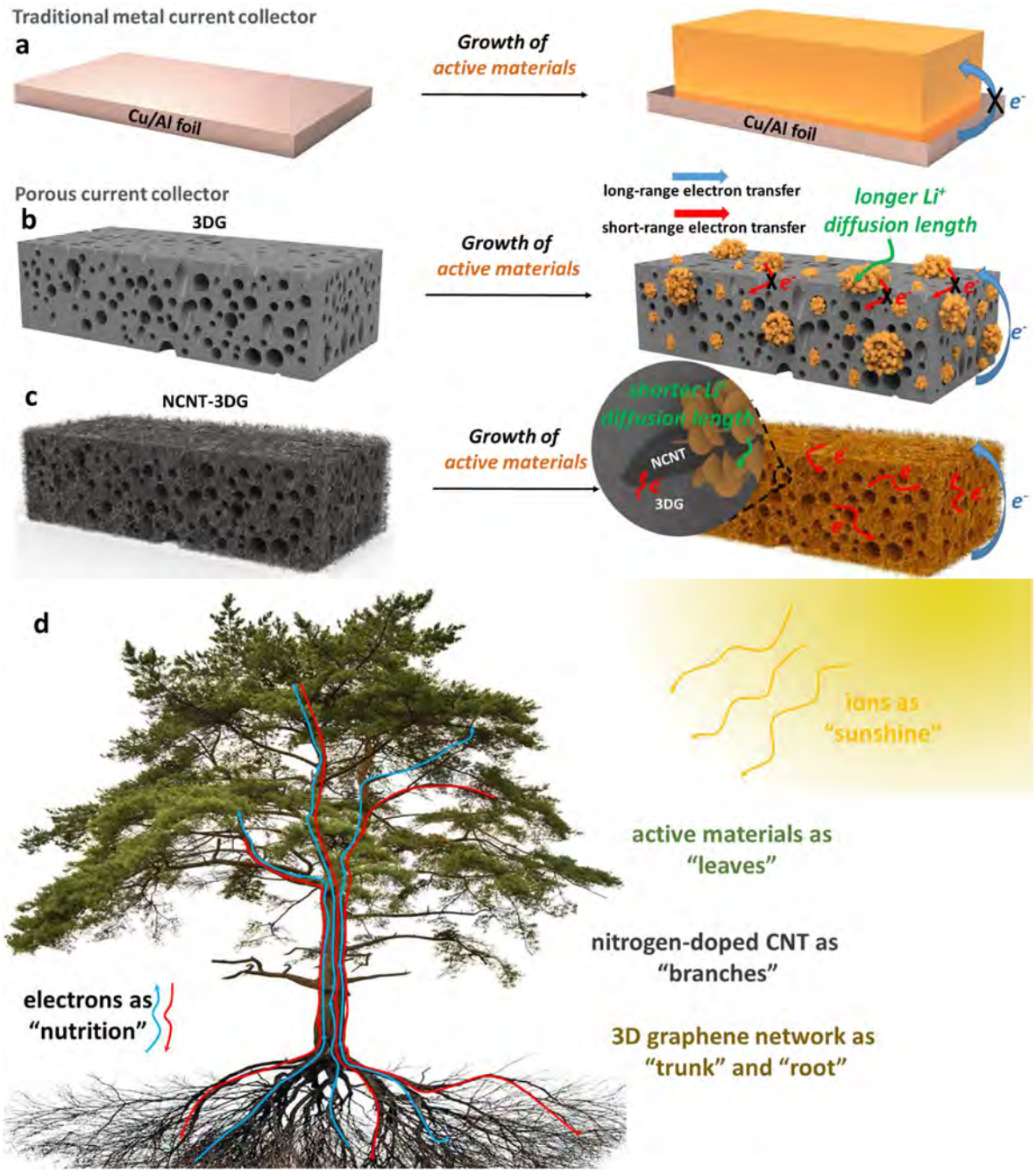

Fig. 1. Schematic illustrating of different growth patterns of active materials on (a) traditional metal current collectors, (b) 3DG and (c) the nitrogen-doped CNT-3DG hybrid (NCNT-3DG). (d) Bio-inspired structure of NCNT-3DG with active materials. (A colour version of this figure can be viewed online.)

chemical reactivity nucleation sites. The presence of both CNTs and the nitrogen induced defects is critically important for creating a good platform for uniform deposition of active materials and smooth electron transport across the whole structure. For emphasizing this, contact angle measurements on the surface of CNT-3DG has been conducted (Fig. S2). The latter proved that the contact angle of CNT-3DG (88°) is between that of 3DG and NCNT-3DG. This suggests that the hydrophilicity of the CNT-3DG can be also placed between that of 3DG and NCNT-3DG. As illustrated in Fig. 2c, the freestanding NCNT-3DG hybrid material is flexible.

To control the uniform distribution of NCNT growth within the 3DG, the morphology of $NiCo_2O_4$ was tuned via tailoring the solvothermal process in the solvent mixture by using different volume ratios of water to ethanol. The corresponding morphologies of in-situ growing $NiCo_2O_4$ for volume ratios of water to ethanol 1:0, 1:4, and 0:1, are shown in Fig. 3a, b and c, respectively. Obviously, the solvent mixture has a significant effect on the morphology of $NiCo_2O_4$. It has been already reported that both the dielectric constant and viscosity of the solvent used in a solvothermal process affect the morphology of $NiCo_2O_4$ crystals grown [41–43]. In general, a solvent with lower dielectric constant has been found to reach higher supersaturation and better ion diffusion capabilities, thus allowing more even coating of $NiCo_2O_4$ on 3DG. While solvents with higher viscosity greatly suppress the anisotropic growth of crystals on graphene [41,43]. Ethanol has a lower dielectric constant compared to the water, however ethanol has a higher

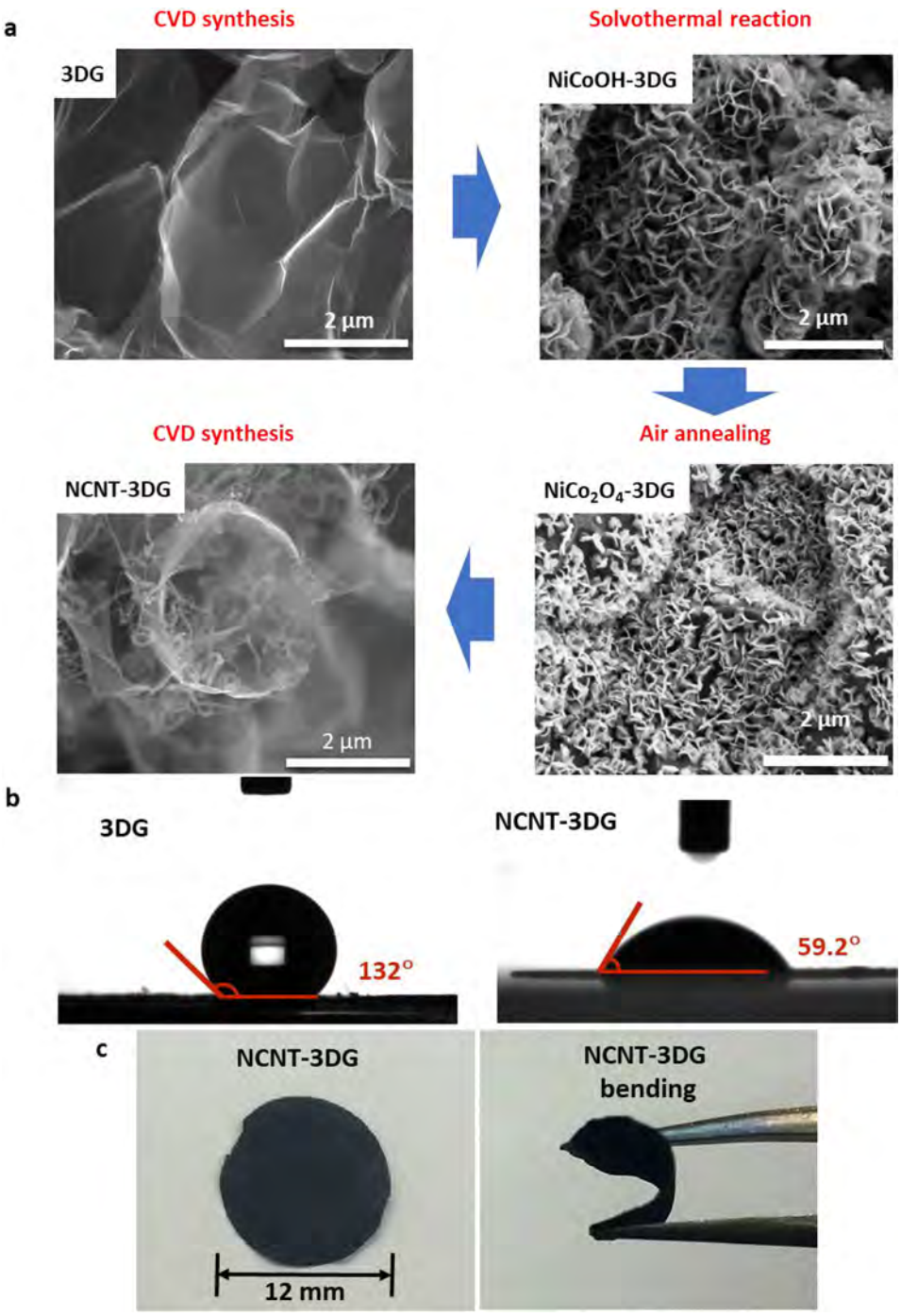

Fig. 2. (a) The illustration of the fabrication process of the NCNT-3DG with top-view SEM images of 3DG, NiCoOH-3DG, NiCo2O4-3DG, and NCNT-3DG. (b) Contact angle test of 3DG and NCNT-3DG using a water droplet. (c) A photograph of the freestanding and flexible NCNT-3DG. (A colour version of this figure can be viewed online.)

viscosity [42]. As shown in Fig. 3a, when pure DI water was used as a solvent, the "as-grown" $NiCo_2O_4$ was unevenly deposited on the 3DG with some cabbage-like microsphere morphology consisted of the nanoflakes with about several hundred nm diameter. However, when solvent pure ethanol was used as a solvent, significant morphological changes have been observed (Fig. 3c). The $NiCo_2O_4$ nanoflakes grown in pure ethanol uniformly cover the 3DG, with cabbage-like microspheres composed of 20 nm in diameter nanoflakes. This is because the dielectric constant of ethanol (23.8) is smaller than the water (78.4) [42], and further causing a better ions diffusion in pure ethanol. Thus, $NiCo_2O_4$ crystals are more likely to grow along the two-dimensional plane. However, the viscosity of ethanol is greater than the DI water, thus suppressing the anisotropic growth of $NiCo_2O_4$. As a result, the $NiCo_2O_4$ cyrstals synthesized in pure ethanol were not perfectly uniform. Therefore, an ethanol-water mixture of 4:1 was chosen to offset the viscosity of the solution while maintaining a relative low dielectric constant. As shown in Fig. 3b, the $NiCo_2O_4$ nanoflakes with similar dimensions grew evenly and vertically on the 3DG. The growth mechanism of the NCNTs in this case of $NiCo_2O_4$ catalyst is known as tip-growth,

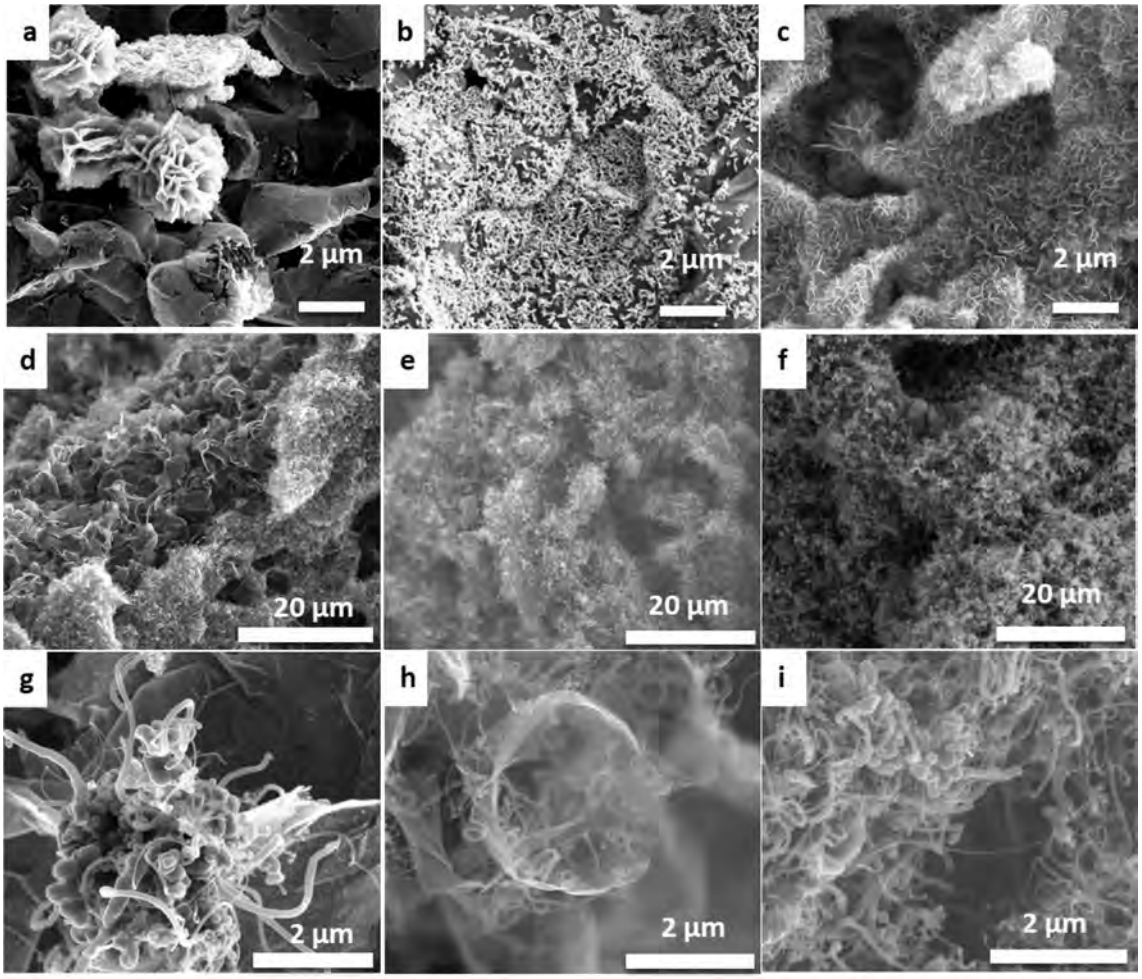

Fig. 3. Top-view SEM images of $NiCo_2O_4$ grown on 3DG during the solvothermal process by using different volume ratios of water to ethanol: (a) 1:0, (b) 1:4, and (c) 0:1, respectively. Top-view SEM images of lower and higher magnification of NCNT-3DG grown on $NiCo_2O_4$ that was synthesized in: (d) (g) pure DI water, (e) (h) 4 to 1 of ethanol to DI water ratio, and (f) (i) pure ethanol.

and the diameter of NCNT is determined by the size of the catalyst particles ($NiCo_2O_4$) [44]. As a consequence, the morphology of $NiCo_2O_4$ has remarkable influence on NCNT growth. SEM images of NCNT grown from a $NiCo_2O_4$ catalyst prepared via pure ethanol and pure DI water solvent are shown in Fig. 3d and g, and Fig. 3f and i, respectively. In the case of NCNTs grown on $NiCo_2O_4$ prepared via pure DI water, the distribution and shape of the NCNTs are not uniform, because some $NiCo_2O_4$ aggregates are accumulated locally on the 3DG due to lower viscosity of pure DI water (Fig. 3d, g). On the contrary, the NCNTs grown on $NiCo_2O_4$ nanoflakes and microspheres produced via pure ethanol revealed uniform growth all over the 3DG, but the NCNTs were with various dimensions in term of length and diameter (Fig. 3f, i). To grow uniformly distributed NCNTs with similar diameters, the ethanol solution was modified with 1:4 vol ratio of water to ethanol. As shown in Fig. 3e, h, the NCNTs not only grew uniformly within the 3DG but also with similar diameters. This structure is expected to be an ideal current collector platform for loading of active materials. Also, the NCNTs distribute uniformly within the 3DG structure as shown clearly in cross-section view SEM image (Fig. S3), which is attributed to the optimized values of dielectric constant and viscosity to cause the even distribution of $NiCo_2O_4$ nanoflakes with similar dimensions within the 3DG structure.

The morphology of the NCNT-3DG was further analyzed by TEM. As shown in Fig. 4a, the hybrid materials consist of transparent graphene flasks and abundant NCNTs with 20–50 nm in diameter. From the higher magnification of TEM images (inset in Fig. 4a), the tips of NCNTs are opened, which is expected to offer more space for active materials. This could be the potential feature to limit the huge volume change of silicon anode in LIB. Fig. 4b displays Raman spectra of the 3DG and the NCNT-3DG. In general, when interpreting the Raman spectra of graphene, the D peak at about 1350 cm^{-1} usually suggests defects or carbon with sp^3 bond [45]. The I_G/I_D ratio is reduced from 22.2 in pristine 3DG to 1.8 in the NCNT-3DG, suggesting a higher defect concentration in the NCNT-3DG due to nitrogen-induced defects. To confirm the surface chemistry of the NCNT-3DG, XPS was employed, and the results are shown in Fig. 4c and d, where all spectra were calibrated by setting the peak in the C 1s to the sp^2 carbons at 284.5 eV. The survey scan in Fig. 4c proves that the CNTs growth with assistance of acetonitrile during CVD, introduces nitrogen with concentration in the NCNTs of 2.5 at%. The high-resolution N 1s spectrum of the NCNT-3DG (Fig. 4d) reveals four different N-doping forms including pyridinic N (398.1 eV), pyrrolic N (400.3 eV), quaternary N (403.3 eV), and N oxide (404.1 eV) [46,47]. The pyrrolic and quaternary N (also called graphitic N) functional groups specifically have been shown to improve the electrochemical performance of the N doped carbon based materials [46].

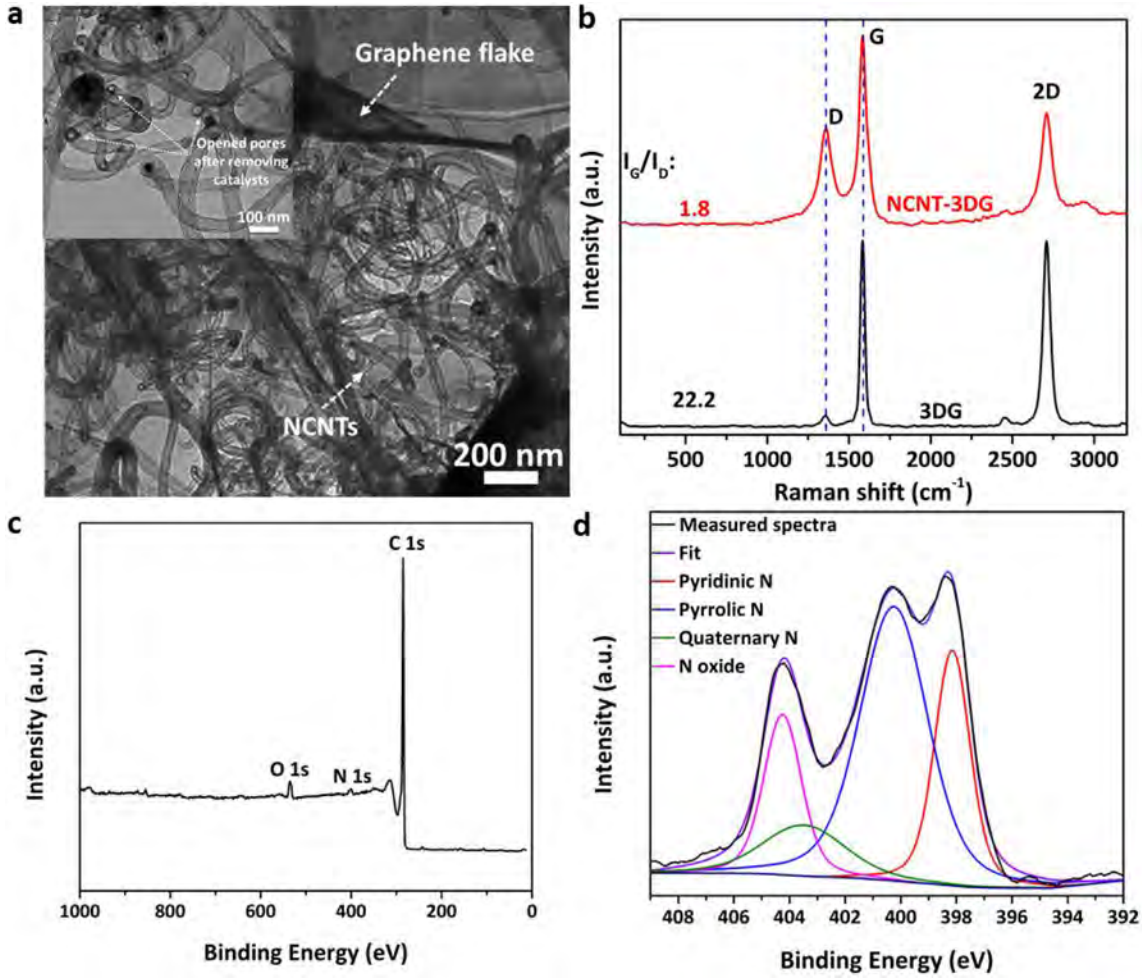

Fig. 4. (a) TEM image of NCNT-3DG. (b) Raman spectra of 3DG and NCNT-3 DG. (c) XPS survey spectrum of NCNT-3DG. (d) High resolution XPS spectrum of N 1s. (A colour version of this figure can be viewed online.)

3.2. Preparation and characterization of LTO-3DG and LTO-NCNT-3DG composite electrodes

The LTO-3DG and the LTO-NCNT-3DG electrodes were fabricated by the hydrothermal deposition of active materials on the 3DG and NCNT-3DG followed by annealing in argon. Both 3DG and NCNT-3DG were directly used as highly conductive networks for electrons/lithium ions and current collectors without using any binder, conductive additive or metal current collector. After introducing nitrogen-doped CNT, the composite became more hydrophilic compared to the pristine 3DG, because the pronounced wettability difference between 3DG and NCNT-3DG. As a result, the morphologies of LTO on 3DG and on NCNT-3DG were obviously different. Morphological features of the LTO-3DG and the LTO-NCNT-3DG are shown in Fig. 5a and b. The 3DG shows hydrophobic nature that leads to agglomeration and non-uniformity of the active materials (LTO) (Fig. 5a). To further elaborate the positive connection between the presence of CNTs with nitrogen doping and the distribution of active materials, samples without nitrogen doping (LTO-CNT-3DG) have been synthesized. As shown in Fig. S4, the morphology of LTO on the CNT-3DG is slightly more uniform than that of the 3DG, however still with some agglomerations. Obviously, the lack of nitrogen doped sites in the CNT-3DG causes the LTO nanoflakes not to be deposited uniformly on the entire nanotubes. However, the NCNT-3DG hybrid structure combining the defective NCNT with the 3DG prevents the active materials to agglomerate thus forming a uniform coating of LTO nanoflakes with a few nanometers in thickness (Fig. 5b). This morphology is ideal for achieving faster long-range and short-range electron transfer, and faster lithium ions insertion/extraction. The NCNT-3DG possessing nucleation sites with higher chemical reactivity allows the LTO nanoflakes to be deposited uniformly on the NCNT-3DG which enables better contact and stronger binding between LTO nanoflakes and the NCNT-3DG with no need of any binder. The contact angle and electrical conductivity measurements demonstrated that nitrogen doping of the NCNT-3DG not only increased the electrical conductivity but also improved the wettability between NCNT-3DG and the aqueous solution. The LTO-NCNT-3DG has been employed as a freestanding electrode without the use of any polymeric binders (Fig. S5). It also revealed a reasonable mechanical strength of 6.2 MPa at a strain of 1.89%. The obtained strength value suggests that the synthesized LTO-NCNT-3DG possesses a good mechanical stability.

The XRD pattern of the LTO-NCNT-3DG and LTO-3DG (Fig. 6a) showed a clear peak at around 26°, which can be attributed to the (002) reflection of 3DG in both samples. All the other peaks of the two samples were in accordance with the cubic spinel $Li_4Ti_5O_{12}$ (JCPDS NO.49–0207) [48], indicating a high crystallinity of the LTO nanoflakes. Raman spectra of the LTO-NCNT-3DG and LTO-3DG were conducted to affirm the successful synthesis of LTO on both

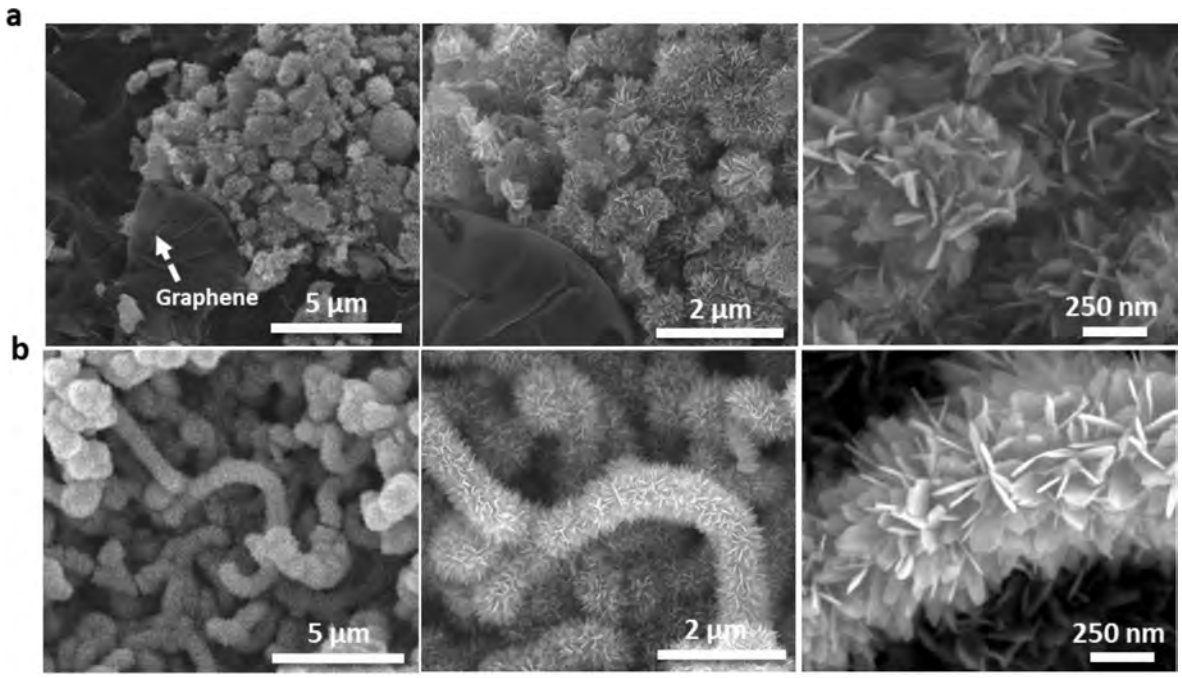

Fig. 5. Top-view SEM images of (a) LTO-3DG and (b) LTO- NCNT-3DG.

NCNT-3DG and 3DG carbon nanostructured current collectors. As shown in Fig. 6b, the two composites showed characteristic peaks of $Li_4Ti_5O_{12}$ observed between 100 and 1000 cm^{-1} [48,49]. Besides, the peaks observed at 1350 and 1583 cm^{-1} were attributed to the D and G bands of the disordered and the ordered graphitic carbons [18,29]. The surface elemental composition of the LTO-NCNT-3DG was confirmed by XPS analysis. The survey spectrum shows the presence of O 1s, Ti 2p, C 1s, N 1s, and Li 1s in the composite (Fig. S6). The high resolution XPS spectra for different species in the LTO-NCNT-3DG are displayed in Fig. 6c–f. The high-resolution scan for Ti shows mainly two peaks from the corresponding Ti^{4+} species at approximately 465 eV (Ti $2p_{1/2}$) and 459 eV (Ti $2p_{3/2}$) binding energies (Fig. 6c) [48]. During the carbonization process, Ti^{4+} gets reduced to Ti^{3+} which leads to improved electrical conductivity of LTO material. A small peak belonging to Ti 3p (Ti^{4+}) was also observed around 65 eV as shown in the survey spectrum in Fig. S6. The O 1s (Fig. 6d) reveals Ti–O, C–O and C=O species which represent the oxidized state of titanium and carbon in the LTO-NCNT-3DG material respectively [29,50]. In case of C 1s (Fig. 6e), a major peak at 284.6 eV belonging to C–C (sp^2) was observed indicating the graphitic structure of the material [50]. The other prominent peak belongs to sp^3 type carbon which includes C–N and C–OH type of species [50]. Other small peaks in the spectrum there correspond to C=O and COOH, respectively [50]. The N 1s (Fig. 6f) shows three main characteristic peaks belonging to pyridinic, pyrrolic and quaternary N species at approximately 398 eV, 400 eV and 401 eV, respectively [46,47]. These species, as mentioned above in the previous XPS analysis section for the NCNT-3DG material, have been shown to improve the electrochemical performance by creating a greater number of electron rich active sites in the material [46].

3.3. Electrochemical performance

To investigate the electrochemical performance of the LTO-NCNT-3DG electrode, compare it with that of the LTO-3DG electrode was performed. The NCNT-3DG was rationally designed, the LTO-NCNT-3DG with LTO nanoflakes well anchored within the NCNT-3DG scaffold, the electrochemical performance of the monolithic LTO-NCNT-3DG composite is apparently facilitated. The cyclic voltammetry (CV) curves of the LTO-3DG and LTO-NCNT-3DG at scan rate of 0.2 mV s^{-1} in the range of 1.0–2.5 V (vs. Li/Li^+) are shown in Fig. 7a. LTO-3DG and LTO-NCNT-3DG electrodes both have a pair of oxidation and reduction peaks at about 1.55 V, corresponding to the characteristic peaks of the reversible phase transformation between $Li_4Ti_5O_{12}$ and $Li_7Ti_5O_{12}$. [6,48] It was revealed that the potential interval between the anodic and cathodic peaks of LTO-NCNT-3DG was 122 mV, which was much smaller than 261 mV for the LTO-3DG. This signifies that the LTO-NCNT-3DG has lower polarization due to a good electrical conductivity of the overall electrode promoting the electrochemical performance of the composite [51,52]. Moreover, the redox peak profile of LTO-NCNT-3DG was sharper, larger and more symmetric than that of LTO-3DG, suggesting that the redox kinetics and reversible capacity were improved due to a faster Li ions diffusion and a more smooth transport of electrons [8,48]. Additionally, the CV curves of LTO-3DG and LTO-NCNT-3DG at different scan rates are displayed in Fig. S7. It was noted that the redox peaks of both samples demonstrate a linear relationship between the peak currents and the square root of the scan rates, suggesting a diffusion-controlled process [8,53]. The diffusion coefficient of Li ions calculated from the slope (K values shown in the insets of Fig. S7) of the charge-discharge process for the LTO-NCNT-3DG was greater than that for the LTO-3DG. This suggests a faster diffusion rate of Li ions in the LTO-NCNT-3DG over the LTO-3DG.

The effect of the two different carbon current collectors on the reaction kinetics of electrode performances was further studied by electrochemical impedance spectroscopy (EIS). The related Nyquist plots are shown in Fig. 7b. This data showed that the charge transfer resistance of the LTO-NCNT-3DG (13.8 Ω) was lower than that of the LTO-3DG (30.1 Ω), suggesting a faster Li ions charge transfer of the LTO-NCNT-3DG. The latter could be a result of the uniform distribution of LTO nanoflakes thanks to the nitrogen doping. This phenomenon is in agreement with the results observed in the CV

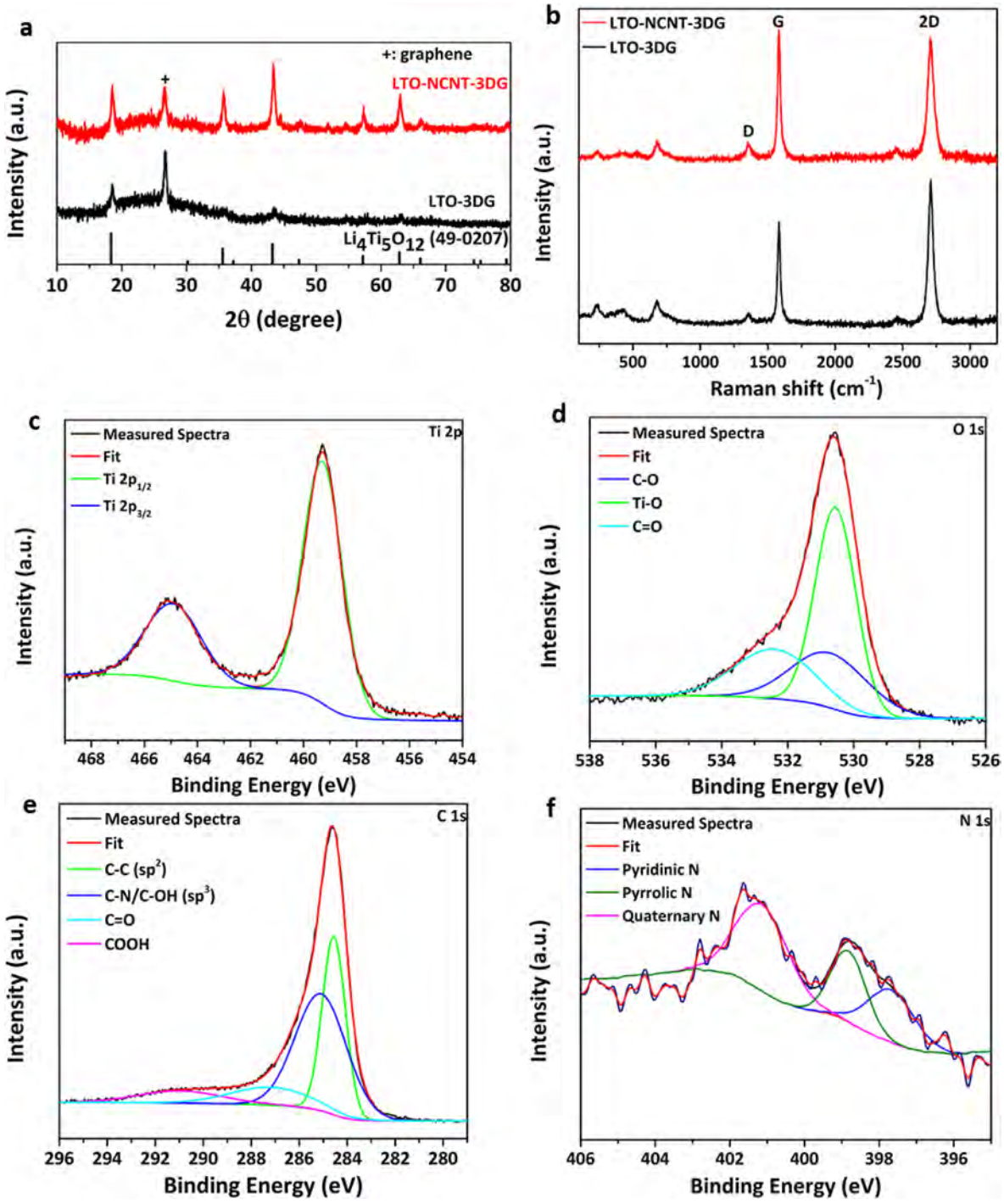

Fig. 6. (a) XRD of LTO-3DG and LTO-NCNT-3DG, (b) Raman of LTO-3DG and LTO-NCNT-3DG. (c) XPS analysis of LTO-NCNT-3DG (c) Ti 2p, (d) O 1s, (e) C 1s, and (f) N 1s. (A colour version of this figure can be viewed online.)

curves. Further, the LTO-NCNT-3DG showed a smaller intercept on the real axis than the LTO-3DG, indicating a lower electronic resistance. This could be attributed to an improved electronic conductivity over the whole structure because of the seamless assebling of 3DG and NCNTs and the good attachment of the LTO nanoflakes on the NCNTs. The integrated conductive network (NCNT-3DG) is favorable for faster Li ions diffusion and electrons transport, so the utilization of active materials is enhanced, resulting in better reaction kinetics. The inset of Fig. 7b shows the equivalent circuit for the EIS plots. Rs represents the bulk resistance of the electrolyte, separator and the electrode, the (C1-R1) parallel circuit segment corresponds to the second electron interface film, electrode roughness and the inhomogeneous reaction at the surface. The Rct-CPE-Zw parallel segment takes into account the interface charge transfer process, and the Warburg diffusion [54,55].

The galvanostatic charge-discharge behavior of the LTO-3DG and LTO-NCNT-3DG were evaluated at different C-rates between 1.0 and 2.5 V versus Li^+/Li^0, as displayed in Fig. 7c and d, respectively. Both electrodes have a pair of flat plateaus, representing the

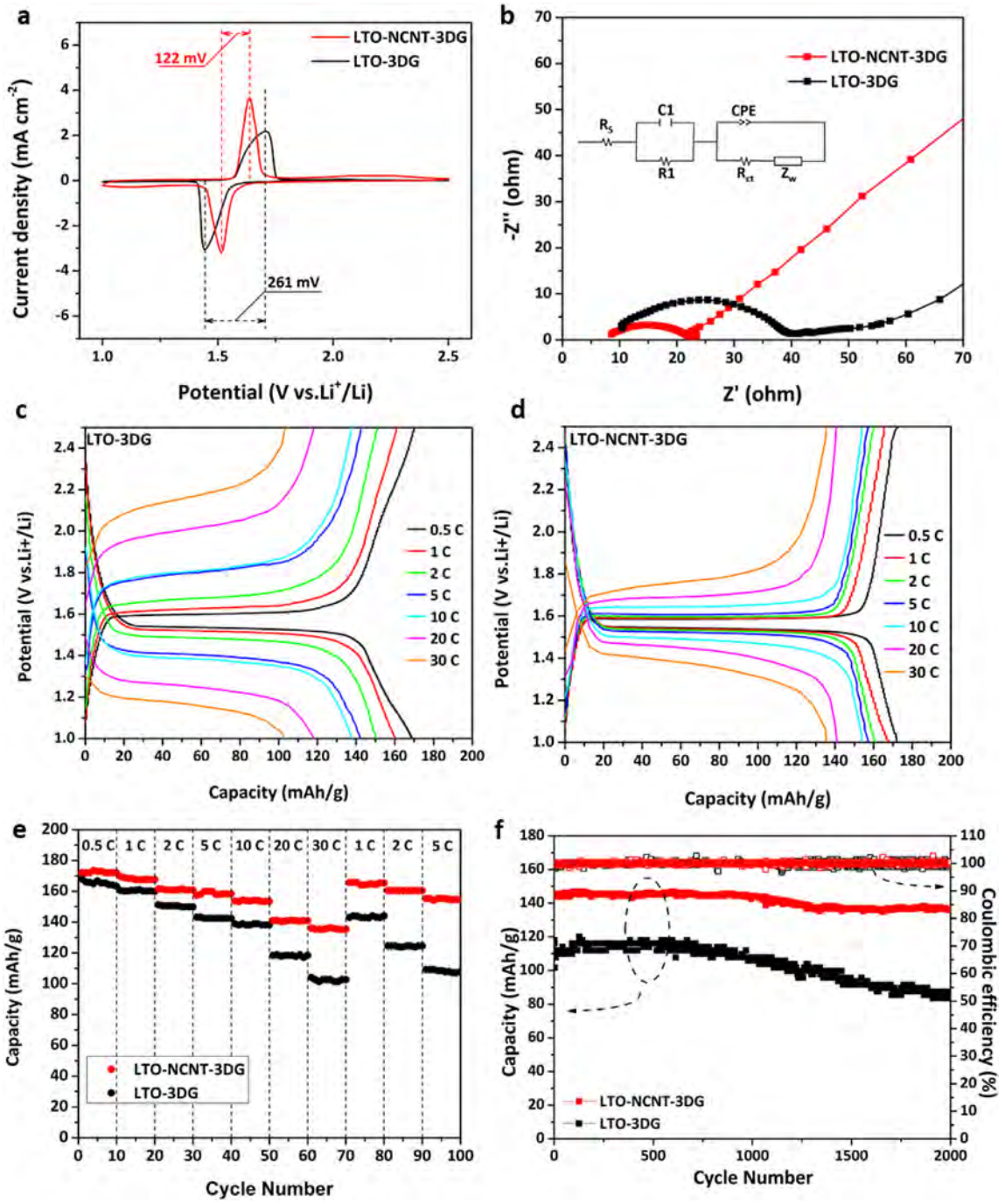

Fig. 7. Electrochemical characterization of LTO-3DG and LTO-NC NT-3DG: (a) CV curves at a scan rate of 0.2 mV s^{-1}; (b) EIS spectra. Charge-discharge profiles of: (c) LTO-3DG; (d) LTO-NCNT-3DG at different current densities; (e) Rate performance; (f) Cycling performance at a current density of 10 C for 2000 cycles. (A colour version of this figure can be viewed online.)

insertion/extraction behavior of Li ions in/out LTO [8,17]. Although the LTO-3DG and the LTO-NCNT-3DG have similar specific capacities at 0.5C, with further increase of C-rate, the charge-discharge potential plateaus of LTO-NCNT-3DG were more stable and longer than that of the LTO-3DG. The LTO-NCNT-3DG showed a discharge capacity of 157, 154 and 142 mAh g^{-1} at 5, 10 and 20 C, respectively, while LTO-3DG revealed 142, 137, and 118 mAh g^{-1} at the corresponding rates. The potential differences between charge and discharge of the LTO-3DG and LTO-NCNT-3DG at each C-rate are compared in Fig. S8. Obviously, the LTO-NCNT-3DG shows lower potential differences at various C-rates, indicating higher electrochemical reversibility and smaller polarization. The rate performances of the LTO-3DG and LTO-NCNT-3DG electrodes were evaluated by increasing the charge-discharge current density stepwise from 0.5C to 30 C at every 10 cycles. As displayed in Fig. 7e, the LTO-NCNT-3DG delivered a capacity of 172 mAh g^{-1} to 135 mAh g^{-1}, with retention of 79%, when the C-rate increased from 0.5C to 30 C. In contrast, the LTO-3DG only showed a retention of 61%, suggesting that more serious polarization occurred in the LTO-3DG. Additional comparison of the LTO-NCNT-3DG with the LTO-3DG

showed further superiority of the NCNTs containing electrode in terms of high reversible capacity of 166 mAh g^{-1} and retention of 97% that can be achieved when the C-rate is returned from 30 to 1 C. All this demonstrated an excellent high rate cycling stability due to the reasonable combination of NCNTs and 3DG. Fig. 7f shows the cyclic performance of the LTO-3DG and LTO-NCNT-3DG at 10 C. The reversible capacity of the LTO-NCNT-3DG remained at 136 mAh g^{-1} after 2000 cycles with a capacity retention of 94%. The cycling stability of LTO-NCNT-3DG was also superior to the LTO-3DG, which only delivered a reversible capacity of 83 mAh g^{-1} with a capacity retention of 70% under the same testing conditions. The better cyclability of LTO-NCNT-3DG is attributed to the good mechanical robustness of NCNT-3DG. Table 1 shows a comparison of the performance for the LTO-NCNT-3DG electrode designed and created in this work to other LTO-based electrode described in the literature [8,17,28,31,48,49,51,53,56–59]. Most of literature does not consider the weight of the current collector or the binder, which results in an over-estimated LTO content in the cell. Our free-standing LTO-NCNT-3DG electrode was made without any binder, conductive additive, or metal current collector, thus securing a high actual LTO content of 74 wt%. This allowed to achieve a good cycle life with 94% capacity retention after 2000 cycles at 10 C. In summary, the improved electrochemical performance of LTO-NCNT-3DG can be interpreting by the following factors. First, electronic conductivity of the overall electrode is enhanced by the combination of NCNT and 3DG, which provides a highly conductive pathway for electrons across the whole macrostructure during high rate operation. Second, the intimate contact between LTO nanoflakes and NCNT-3DG mitigates the inner resistance between the two components, which was beneficial for the observed fluent electron transfer. Third, compared with the pristine 3DG, the NCNT-3DG with nitrogen doping provide a hydrophilic surface with increased wettability. This allowed LTO nanoflakes to be deposited uniformly on the NCNT-3DG, rather than forming the agglomeration of the relatively bulky LTO particles on the pristine 3DG. The uniform distribution of LTO nanoflakes in the LTO-NCNT-3DG with higher specific surface area not only shortens the Li ions transporting pathway, but also reduces local current density. The resulting effect minimizies the polarization and facilitating favorable electrode reaction kinetic [60].

4. Conclusions

A bio-inspired, amphiphilic hybrid material consisted of nitrogen-doped CNT-three-dimensional graphene (NCNT-3DG) has been successfully synthesized and characterized. The obtained material has been employed as a novel current collector for loading $Li_4Ti_5O_{12}$ (LTO). The NCNT-3DG current collector offers a high electrical conductivity (421 S cm^{-1}) that compensates the low electrical conductivity of LTO (<10^{-13} S cm^{-1}). The obtained NCNT-3DG hybrid material provides fast electron transfer and mechanical robustness. It also offers more hydrophilic sites though the NCNTs for uniform loading of active materials in a monolithic structure free of any metal current collector or binder. This hybrid material has smaller junction resistance between NCNT and 3DG and greater chemical reactivity nucleation sites, facilitating high mass loading of the LTO without any delamination. The NCNTs in the NCNT-3DG is hydrophilic, thus preventing the agglomeration of LTO which is deposited as a uniform coating. This hybrid structure is ideal for achieving high electrical conductivity in a long-range and short-range term and faster lithium ion insertion and extraction. The LTO-NCNT-3DG material showed superior electrochemical performance, higher specific capacity, better rate performance and an improved cycling performance compared to the LTO-3DG. Further comparison revealed that the LTO-NCNT-3DG electrode has a lower polarization, lower charge transfer resistance, better capacitance retention, improved redox kinetics and reversible capacitance, contributing to its improved electrochemical performance. The

Table 1
Comparison of cycling and rate performances of the LTO-NCNT-3DG with other LTO-based electrodes in the literature.

Materials of electrodes	Active materials/all components[a] in electrode (wt %); Active materials (mg cm^{-2})	Current rate (C)	Cycle number	Initial specific capacity (mAh g^{-1})	Capacity retention (%)	Ref.
LTO-NCNT-3DG	74; 2	10	2000	145	94	This work
LTO-N-C	98 (w/o current collector); 2	5	/	153	/	[48]
LTO-C	14; 1.31	5	3000	162.5	74	[56]
G-LTO-CNT	62.5 (w/o carbon cloth); /	20	10000	150	89.5	[28]
LTO-rGO	76 (w/o copper foil); /	10	/	175	/	[8]
LTO-C	14.8–17.5; 1.4–1.7	10	200	170.2	77.5	[51]
LTO	77.4 (w/o current collector); 2	10	500	151.1	92.6	[31]
LTO-CNT	77.5; 3.2	10	1200	134.3	63.5	[49]
LTO	80 (w/o copper foil); /	15	/	148	/	[53]
LTO-G	79.6 (w/o copper foil); /	10	1000	74.8	71.4	[57]
LTO-G	77.2 (w/o copper foil); /	10	500	162.5	90.3	[58]
LTO-CNT	56; /	5.7 (1A g^{-1})	8000	103	88.8	[61]
LTO-G	77.9 (w/o copper foil); /	0.5	100	177	89.8	[62]

[a] All components including active material/composite, conductive additive, binder and current collector. Areal density of NCNT-3DG: 0.7 mg cm^{-2}, and of copper foil ~8 mg cm^{-2}.

presented work here can be considered as part of the LIB community efforts to design and create the next-generation current collector superior to the existing electrode materials.

Acknowledgement

The authors acknowledge the financial support from the NASA [grant NNC16CA17C].

Appendix A. Supplementary data

Supplementary data to this article can be found online at https://doi.org/10.1016/j.carbon.2019.01.055.

References

[1] X.L. Wu, L.Y. Jiang, F.F. Cao, Y.G. Guo, L.J. Wan, LiFePO4 nanoparticles embedded in a nanoporous carbon matrix: superior cathode material for electrochemical energy-storage devices, Adv. Mater. 21 (2009) 2710–2714, https://doi.org/10.1002/adma.200802998.
[2] N. Armaroli, V. Balzani, Towards an electricity-powered world, Energy Environ. Sci. 4 (2011) 3193–3222, https://doi.org/10.1039/C1EE01249E.
[3] S. Ahmed, I. Bloom, A.N. Jansen, T. Tanim, E.J. Dufek, A. Pesaran, A. Burnham, R.B. Carlson, F. Dias, K. Hardy, M. Keyser, C. Kreuzer, A. Markel, A. Meintz, C. Michelbacher, M. Mohanpurkar, P.A. Nelson, D.C. Robertson, D. Scoffield, M. Shirk, T. Stephens, R. Vijayagopal, J. Zhang, Enabling fast charging – a battery technology gap assessment, J. Power Sources 367 (2017) 250–262, https://doi.org/10.1016/j.jpowsour.2017.06.055.
[4] H. Zhang, X. Yu, P.V. Braun, Three-dimensional bicontinuous ultrafast-charge and-discharge bulk battery electrodes, Nat. Nanotechnol. 6 (2011) 277–281, https://doi.org/10.1038/nnano.2011.38.
[5] D.P. Singh, F.M. Mulder, A.M. Abdelkader, M. Wagemaker, Facile micro templating LiFePO4 electrodes for high performance Li-ion batteries, Adv. Energy Mater. 3 (2013) 572–578, https://doi.org/10.1002/aenm.201200704.
[6] N. Li, Z. Chen, W. Ren, F. Li, H.-M. Cheng, Flexible graphene-based lithium ion batteries with ultrafast charge and discharge rates, Proc. Natl. Acad. Sci. Unit. States Am. 109 (2012) 17360–17365, https://doi.org/10.1073/pnas.1210072109.
[7] B. Wang, W. Al Abdulla, D. Wang, X.S. Zhao, A three-dimensional porous LiFePO4 cathode material modified with a nitrogen-doped graphene aerogel for high-power lithium ion batteries, Energy Environ. Sci. 8 (2015) 869–875, https://doi.org/10.1039/C4EE03825H.
[8] H. Ge, T. Hao, H. Osgood, B. Zhang, L. Chen, L. Cui, X.M. Song, O. Ogoke, G. Wu, Advanced mesoporous spinel Li4Ti5O12/rGO composites with increased surface lithium storage capability for high-power lithium-ion batteries, ACS Appl. Mater. Interfaces 8 (2016) 9162–9169, https://doi.org/10.1021/acsami.6b01644.
[9] Y. Yamada, K. Furukawa, K. Sodeyama, K. Kikuchi, M. Yaegashi, Y. Tateyama, A. Yamada, Unusual stability of acetonitrile-based superconcentrated electrolytes for fast-charging lithium-ion batteries, J. Am. Chem. Soc. 136 (2014) 5039–5046, https://doi.org/10.1021/ja412807w.
[10] H. Wu, D. Zhuo, D. Kong, Y. Cui, Improving battery safety by early detection of internal shorting with a bifunctional separator, Nat. Commun. 5 (2014) 1–6, https://doi.org/10.1038/ncomms6193.
[11] J.H. Kim, M. Gu, D.H. Lee, J.H. Kim, Y.S. Oh, S.H. Min, B.S. Kim, S.Y. Lee, Functionalized nanocellulose-integrated heterolayered nanomats toward smart battery separators, Nano Lett. 16 (2016) 5533–5541, https://doi.org/10.1021/acs.nanolett.6b02069.
[12] J.-Q. Huang, H.-J. Peng, X.-Y. Liu, J.-Q. Nie, X.-B. Cheng, Q. Zhang, F. Wei, Flexible all-carbon interlinked nanoarchitectures as cathode scaffolds for high-rate lithium–sulfur batteries, J. Mater. Chem. A. 2 (2014) 10869, https://doi.org/10.1039/c4ta00245h.
[13] Z. Yuan, H.J. Peng, J.Q. Huang, X.Y. Liu, D.W. Wang, X.B. Cheng, Q. Zhang, Hierarchical free-standing carbon-nanotube paper electrodes with ultrahigh sulfur-loading for lithium-sulfur batteries, Adv. Funct. Mater. 24 (2014) 6105–6112, https://doi.org/10.1002/adfm.201401501.
[14] G. Hu, C. Xu, Z. Sun, S. Wang, H.M. Cheng, F. Li, W. Ren, 3D graphene-foam-reduced-graphene-oxide hybrid nested hierarchical networks for high-performance Li-S batteries, Adv. Mater. 28 (2016) 1603–1609, https://doi.org/10.1002/adma.201504765.
[15] S.H. Chung, A. Manthiram, Low-cost, porous carbon current collector with high sulfur loading for lithium-sulfur batteries, Electrochem. Commun. 38 (2014) 91–95, https://doi.org/10.1016/j.elecom.2013.11.008.
[16] L. Sun, W. Kong, H. Wu, Y. Wu, D. Wang, F. Zhao, K. Jiang, Q. Li, J. Wang, S. Fan, Mesoporous Li $_4$ Ti $_5$ O $_{12}$ nanoclusters anchored on super-aligned carbon nanotubes as high performance electrodes for lithium ion batteries, Nanoscale 8 (2016) 617–625, https://doi.org/10.1039/C5NR06406F.
[17] X. Jia, Y. Kan, X. Zhu, G. Ning, Y. Lu, F. Wei, Building flexible Li4Ti5O12/CNT lithium-ion battery anodes with superior rate performance and ultralong cycling stability, Nano Energy 10 (2014) 344–352, https://doi.org/10.1016/j.nanoen.2014.10.012.
[18] W. Chen, H. Jiang, Y. Hu, Y. Dai, C. Li, Mesoporous single crystals Li4Ti5O12 grown on rGO as high-rate anode materials for lithium-ion batteries, Chem. Commun. 50 (2014) 8856–8859, https://doi.org/10.1039/C4CC02886D.
[19] B.P. Vinayan, R. Nagar, V. Raman, N. Rajalakshmi, K.S. Dhathathreyan, S. Ramaprabhu, Synthesis of graphene-multiwalled carbon nanotubes hybrid nanostructure by strengthened electrostatic interaction and its lithium ion battery application, J. Mater. Chem. 22 (2012) 9949, https://doi.org/10.1039/c2jm16294f.
[20] S. Chen, P. Chen, Y. Wang, Carbon nanotubes grown in situ on graphene nanosheets as superior anodes for Li-ion batteries, Nanoscale 3 (2011) 4323, https://doi.org/10.1039/c1nr10642b.
[21] S. Li, Y. Luo, W. Lv, W. Yu, S. Wu, P. Hou, Q. Yang, Q. Meng, C. Liu, H.M. Cheng, Vertically aligned carbon nanotubes grown on graphene paper as electrodes in lithium-ion batteries and dye-sensitized solar cells, Adv. Energy Mater. 1 (2011) 486–490, https://doi.org/10.1002/aenm.201100001.
[22] Y. Hu, X. Li, J. Wang, R. Li, X. Sun, Free-standing graphene-carbon nanotube hybrid papers used as current collector and binder free anodes for lithium ion batteries, J. Power Sources 237 (2013) 41–46, https://doi.org/10.1016/j.jpowsour.2013.02.065.
[23] S. Chen, W. Yeoh, Q. Liu, G. Wang, Chemical-free synthesis of graphene-carbon nanotube hybrid materials for reversible lithium storage in lithium-ion batteries, Carbon N. Y. 50 (2012) 4557–4565, https://doi.org/10.1016/j.carbon.2012.05.040.
[24] N. Dwivedi, S. Kumar, H.K. Malik, Govind, C.M.S. Rauthan, O.S. Panwar, Correlation of sp3and sp2fraction of carbon with electrical, optical and nano-mechanical properties of argon-diluted diamond-like carbon films, Appl. Surf. Sci. 257 (2011) 6804–6810, https://doi.org/10.1016/j.apsusc.2011.02.134.
[25] C. Mattevi, G. Eda, S. Agnoli, S. Miller, K.A. Mkhoyan, O. Celik, D. Mastrogiovanni, G. Granozzi, E. Carfunkel, M. Chhowalla, Evolution of electrical, chemical, and structural properties of transparent and conducting chemically derived graphene thin films, Adv. Funct. Mater. 19 (2009) 2577–2583, https://doi.org/10.1002/adfm.200900166.
[26] R. Paul, S.N. Das, S. Dalui, R.N. Gayen, R.K. Roy, R. Bhar, A.K. Pal, Synthesis of DLC films with different sp ^{2}/sp ^{3} ratios and their hydrophobic behaviour, J. Phys. D Appl. Phys. 41 (2008), 055309, https://doi.org/10.1088/0022-3727/41/5/055309.
[27] B.L. Coyle, M. Rolandi, F. Baneyx, Carbon-binding designer proteins that discriminate between sp2- and sp3-hybridized carbon surfaces, Langmuir 29 (2013) 4839–4846, https://doi.org/10.1021/la4000846.
[28] Z. Yao, X. Xia, Y. Zhong, Y. Wang, B. Zhang, D. Xie, X. Wang, J. Tu, Y. Huang, Hybrid vertical graphene/lithium titanate-CNTs arrays for lithium ion storage with extraordinary performance, J. Mater. Chem. A. 5 (2017) 8916–8921, https://doi.org/10.1039/c7ta02511d.
[29] J. Liu, A.X. Wei, M. Chen, X. Xia, Rational synthesis of Li4Ti5O12/N-C nanotube arrays as advanced high-rate electrodes for lithium-ion batteries, J. Mater. Chem. A. 6 (2018) 3857–3863, https://doi.org/10.1039/c8ta00312b.
[30] N. Nitta, F. Wu, J.T. Lee, G. Yushin, Li-ion battery materials: present and future, Mater. Today 18 (2015) 252–264, https://doi.org/10.1016/j.mattod.2014.10.040.
[31] C. Wang, S. Wang, L. Tang, Y.B. He, L. Gan, J. Li, H. Du, B. Li, Z. Lin, F. Kang, A robust strategy for crafting monodisperse Li4Ti5O12nanospheres as superior rate anode for lithium ion batteries, Nano Energy 21 (2016) 133–144, https://doi.org/10.1016/j.nanoen.2016.01.005.
[32] L. Zhang, D. DeArmond, N.T. Alvarez, R. Malik, N. Oslin, C. McConnell, P.K. Adusei, Y.-Y. Hsieh, V. Shanov, Flexible micro-supercapacitor based on graphene with 3D structure, Small 13 (2017), https://doi.org/10.1002/smll.201603114, 1603114–na.
[33] J.-H. Bahk, T. Favaloro, A. Shakouri, Thin film thermoelectric characterization techniques, Annu. Rev. Heat Transf. 16 (2013) 51–99, https://doi.org/10.1615/AnnualRevHeatTransfer.v16.30.
[34] Y.-Y. Hsieh, L. Zhang, D. DeArmond, S.N. Kanakaraj, P.K. Adusei, N.T. Alvarez, Y. Fang, J. Daum, V. Shanov, Integrated graphene-sulfur cathode and separator with plasma enhancement for Li-S batteries, Carbon N. Y. 139 (2018) 1093–1103. https://doi.org/10.1016/j.carbon.2018.08.025.
[35] Y.L. Ding, P. Kopold, K. Hahn, P.A. Van Aken, J. Maier, Y. Yu, Facile solid-state growth of 3D well-interconnected nitrogen-rich carbon nanotube-graphene hybrid architectures for lithium-sulfur batteries, Adv. Funct. Mater. 26 (2016) 1112–1119, https://doi.org/10.1002/adfm.201504294.
[36] Q. Zhao, J. Chen, F. Luo, L. Shen, Y. Wang, K. Wu, M. Lu, Assembly of ordered polyaniline-graphene hybrid nanomaterials based on poly(2-methoxyaniline-5-sulfonic acid) functionalized graphene nanosheets, Synth. Met. 221 (2016) 103–113, https://doi.org/10.1016/j.synthmet.2016.08.010.
[37] J.H. Bahk, H. Fang, K. Yazawa, A. Shakouri, Flexible thermoelectric materials and device optimization for wearable energy harvesting, J. Mater. Chem. C. 3 (2015) 10362–10374, https://doi.org/10.1039/c5tc01644d.
[38] S. Mishra, H. Nguyen, P.K. Adusei, Y.-Y. Hsieh, V. Shanov, Plasma enhanced synthesis of N doped vertically aligned carbon nanofibers on 3D graphene, Surf. Interface Anal. (2018) 1–8, https://doi.org/10.1002/sia.6604.
[39] J. Pu, Y. Tong, S. Wang, E. Sheng, Z. Wang, Nickel-cobalt hydroxide nanosheets arrays on Ni foam for pseudocapacitor applications, J. Power Sources 250 (2014) 250–256, https://doi.org/10.1016/j.jpowsour.2013.10.108.
[40] W. Li, L. Xin, X. Xu, Q. Liu, M. Zhang, S. Ding, M. Zhao, X. Lou, Facile synthesis of three-dimensional structured carbon fiber-NiCo2O4-Ni(OH)2high-performance

electrode for pseudocapacitors, Sci. Rep. 5 (2015) 1–6, https://doi.org/10.1038/srep09277.
[41] T. Zhu, J.S. Chen, X.W. Lou, Shape-controlled synthesis of porous Co 3 O 4 nanostructures for application in supercapacitors, Inorg. Chem. 50 (2011) 6482–6492, https://doi.org/10.1039/c0jm00867b.
[42] S. Yin, M. Shinozaki, T. Sato, Synthesis and characterization of wire-like and near-spherical Eu2O3-doped Y2O3 phosphors by solvothermal reaction, J. Lumin. 126 (2007) 427–433, https://doi.org/10.1016/j.jlumin.2006.08.096.
[43] W. Yang, Z. Gao, J. Ma, J. Wang, B. Wang, L. Liu, Effects of solvent on the morphology of nanostructured Co3O4and its application for high-performance supercapacitors, Electrochim. Acta 112 (2013) 378–385, https://doi.org/10.1016/j.electacta.2013.08.056.
[44] S.B.B. Sinnott, R. Andrews, D. Qian, A.M.M. Rao, Z. Mao, E.C.C. Dickey, F. Derbyshire, Model of carbon nanotube growth through chemical vapor deposition, Chem. Phys. Lett. 315 (1999) 25–30, https://doi.org/10.1016/S0009-2614(99)01216-6.
[45] A.C. Ferrari, J.C. Meyer, V. Scardaci, C. Casiraghi, M. Lazzeri, F. Mauri, S. Piscanec, D. Jiang, K.S. Novoselov, S. Roth, A.K. Geim, Raman spectrum of graphene and graphene layers, Phys. Rev. Lett. 97 (2006) 1–4, https://doi.org/10.1103/PhysRevLett.97.187401.
[46] C. Wang, K. Su, W. Wan, H. Guo, H. Zhou, J. Chen, X. Zhang, Y. Huang, High sulfur loading composite wrapped by 3D nitrogen-doped graphene as a cathode material for lithium-sulfur batteries, J. Mater. Chem. A. 2 (2014) 5018–5023, https://doi.org/10.1039/c3ta14921h.
[47] C.M. Chen, Q. Zhang, X.C. Zhao, B. Zhang, Q.Q. Kong, M.G. Yang, Q.H. Yang, M.Z. Wang, Y.G. Yang, R. Schlögl, D.S. Su, Hierarchically aminated graphene honeycombs for electrochemical capacitive energy storage, J. Mater. Chem. 22 (2012) 14076–14084, https://doi.org/10.1039/c2jm31426f.
[48] J. Liu, A.X. Wei, M. Chen, X. Xia, Rational synthesis of $Li_4Ti_5O_{12}$/N-C nanotube arrays as advanced high-rate electrodes for lithium-ion batteries, J. Mater. Chem. A. 6 (2018) 3857–3863, https://doi.org/10.1039/c8ta00312b.
[49] L. Sun, W. Kong, H. Wu, Y. Wu, D. Wang, F. Zhao, K. Jiang, Q. Li, J. Wang, S. Fan, Mesoporous Li4Ti5O12 nanoclusters anchored on super-aligned carbon nanotubes as high performance electrodes for lithium ion batteries, Nanoscale 8 (2016) 617–625, https://doi.org/10.1039/C5NR06406F.
[50] H.R. Byon, B.M. Gallant, S.W. Lee, Y. Shao-Horn, Role of oxygen functional groups in carbon nanotube/graphene freestanding electrodes for high performance lithium batteries, Adv. Funct. Mater. 23 (2013) 1037–1045, https://doi.org/10.1002/adfm.201200697.
[51] D. Mu, Y. Chen, B. Wu, R. Huang, Y. Jiang, L. Li, F. Wu, Nano-sized Li4Ti5O12/C anode material with ultrafast charge/discharge capability for lithium ion batteries, J. Alloy. Comp. 671 (2016) 157–163. https://doi.org/10.1016/j.jallcom.2016.02.095.
[52] Y. Cai, Y. Huang, W. Jia, X. Wang, Y. Guo, D. Jia, Z. Sun, W. Pang, Z. Guo, Super high-rate, long cycle life of europiummodified, carbon-coated, hierarchical mesoporous lithium-titanate anode materials for lithium ion batteries, J. Mater. Chem. A. 4 (2016) 9949–9957, https://doi.org/10.1039/c6ta03162e.
[53] H. Ge, Y. Song, H. Song, H. Tian, X.M. Song, N. Li, S. Wu, D. Liu, X. Gao, X. Shi, Advanced charge performance of pristine Li4Ti5O12spinel for power lithium-ion battery, Ceram. Int. 41 (2015) 3869–3874, https://doi.org/10.1016/j.ceramint.2014.11.065.
[54] S. Yang, X. Feng, K. Müllen, Sandwich-like, graphene-based titania nanosheets with high surface area for fast lithium storage, Adv. Mater. 23 (2011) 3575–3579, https://doi.org/10.1002/adma.201101599.
[55] H. Li, L. Shen, K. Yin, J. Ji, J. Wang, X. Wang, X. Zhang, Facile synthesis of N-doped carbon-coated Li4Ti5O12 microspheres using polydopamine as a carbon source for high rate lithium ion batteries, J. Mater. Chem. A. 1 (2013) 7270–7276, https://doi.org/10.1039/c3ta10623c.
[56] N. Cao, Z. Song, Q. Liang, X. Gao, X. Qin, Hierarchical Li4Ti5O12/C composite for lithium-ion batteries with enhanced rate performance, Electrochim. Acta 235 (2017) 200–209, https://doi.org/10.1016/j.electacta.2017.03.032.
[57] H. Liu, G. Wen, S. Bi, P. Gao, Enhanced rate performance of nanosized $Li_4Ti_5O_{12}$/graphene composites as anode material by a solid state-assembly method, Electrochim. Acta 171 (2015) 114–120, https://doi.org/10.1016/j.electacta.2015.05.008.
[58] Y. Yang, B. Qiao, X. Yang, L. Fang, C. Pan, W. Song, H. Hou, X. Ji, Lithium titanate tailored by cathodically induced graphene for an ultrafast lithium ion battery, Adv. Funct. Mater. 24 (2014) 4349–4356, https://doi.org/10.1002/adfm.201304263.
[59] S.G. Ri, L. Zhan, Y. Wang, L. Zhou, J. Hu, Li4Ti5O12/graphene nanostructure for lithium storage with high-rateperformance, Electrochim. Acta 109 (2013) 389–394, https://doi.org/10.1016/j.electacta.2013.07.059.
[60] J. Wang, H. Zhao, Z. Li, Y. Wen, Q. Xia, Y. Zhang, G. Yushin, Revealing rate limitations in nanocrystalline Li 4 Ti 5 O 12 anodes for high-power lithium ion batteries, Adv. Mater. Interf. 3 (2016) 1600003, https://doi.org/10.1002/admi.201600003.
[61] X. Jia, Y. Kan, X. Zhu, G. Ning, Y. Lu, F. Wei, Building flexible Li4Ti5O12/CNT lithium-ion battery anodes with superior rate performance and ultralong cycling stability, Nano Energy 10 (2014) 344–352. https://doi.org/10.1016/j.nanoen.2014.10.012.
[62] S.G. Ri, L. Zhan, Y. Wang, L. Zhou, J. Hu, H. Liu, Li4Ti5O12/graphene nanostructure for lithium storage with high-rate performance, Electrochim. Acta 109 (2013) 389–394. https://doi.org/10.1016/j.electacta.2013.07.059.